Author Manuscript

Author Manuscript

Author Manuscript

Author Manuscript

HHS Public Access

Author manuscript

Stem Cell Res. Author manuscript; available in PMC 2021 August 12.

Published in final edited form as:

Stem Cell Res. 2021 May ; 53: 102295. doi:10.1016/j.scr.2021.102295.

Matrigel is required for efficient differentiation of isolated, stem cell-derived otic vesicles into inner ear organoids

Sarah Emily Hocevar[a,b], **Liqian Liu**[c], **Robert Keith Duncan**[c,*]

[a]Neuroscience Graduate Program, University of Michigan, Ann Arbor, USA

[b]Department of Biomedical Engineering, University of Michigan, Ann Arbor, USA

[c]Kresge Hearing Research Institute, Department of Otolaryngology-Head & Neck Surgery, University of Michigan, Ann Arbor, USA

Abstract

Inner ear organoids derived from pluripotent stem cells could be a useful model system to study development, disease, and regeneration. However, there is considerable heterogeneity in the size, morphology, and efficiency of organoid production using standard protocols. Greater control of the culture microenvironment could decrease heterogeneity and increase the yield of organoids. Animal-derived otic vesicles show some autonomy during development and can differentiate into cochlear and vestibular domains in mesenchyme-free ex vivo culture. Therefore, we investigated whether stem cell-derived otic vesicles can autonomously generate inner ear organoids. Isolated, stem cell-derived vesicles grew into cyst-like organoids with high efficiency, over 90%, when embedded in droplets of the basement membrane matrix Matrigel. Though nearly all vesicles within the aggregate were competent to mature into organoids, the efficiency of organoid production depended on the stage of vesicle isolation and required supplementation with Matrigel.

Keywords

Inner ear; Organoid; Stem cell; Differentiation; Hair cell; Matrigel

1. Introduction

Recent advances in stem cell biology have produced a shift in attention toward in vitro models of organogenesis. By incorporating principles of developmental biology with three-dimensional culture paradigms, these cultures can form complex, multicellular organoids

This is an open access article under the CC BY-NC-ND license (http://creativecommons.org/licenses/by-nc-nd/4.0/).

*Corresponding author at: Kresge Hearing Research Institute, University of Michigan, 1150 W. Medical Center Drive, 5323 Med Sci I, Ann Arbor, MI 48109-5616, USA. rkduncan@umich.edu (R.K. Duncan).

Declaration of Competing Interest

The authors declare that they have no known competing financial interests or personal relationships that could have appeared to influence the work reported in this paper.

Appendix A. Supplementary data

Supplementary data to this article can be found online at https://doi.org/10.1016/j.scr.2021.102295.

Author Manuscript Author Manuscript Author Manuscript Author Manuscript

that resemble a variety of organ systems. Small changes in the timing and type of applied chemical cues lead to organoids with diverse features, including those characteristic of lung (Dye et al., 2015), kidney (Taguchi et al., 2014), intestine (Spence et al., 2011), stomach (McCracken et al., 2014), retina (Eiraku et al., 2011), brain (Eiraku et al., 2008), and the inner ear (Koehler et al., 2013). While organoids have the potential to unlock mysteries in both basic and translational sciences, heterogeneity, poor reproducibility, and inefficiency remain major roadblocks (Huch et al., 2017).

One of the most common protocols for deriving tissues of ectodermal origin begins with the serum-free formation of embryoid bodies from pluripotent stem cells, where culture conditions suppress the formation of other germ layers with varying degrees of success (Eiraku et al., 2008, Koehler et al., 2013). The result is a heterotypic aggregation of organoid cells along with other cell types. For example, both optic and otic organoids are derived from vesicular intermediates surrounded by mesenchyme and a large number of unspecified cells. The role that extra-organoid cells play in organoid-genesis remains uncertain. For optic vesicles, the surrounding non-retinal neuroectoderm appears necessary for organoid production. Isolated cultures of optic vesicles matured into retinal organoids only when non-retinal neuroectoderm was included. Thus, optic vesicles are non-autonomous for organoid-genesis, requiring the adjacent non-retinal cells to provide morphogens for maturation (Eiraku et al., 2011). It remains unclear whether otic vesicle (OV) intermediates also require surrounding mesenchymal cells for development into inner ear organoids.

All sensory and non-sensory components of the inner ear are derived from native OVs. Thus, if stem cell-derived OVs are able to mature autonomously, progenitors in these OVs could be ideal donor material for implantation into the damaged ear and could serve as a useful model system for studying development under controlled culture conditions. Animal-derived OVs show some autonomy in organogenesis, differentiating in ex vivo culture into vestibular and cochlear domains under mesenchyme-free conditions (Miura et al., 2004). In this study, we sought to examine whether OVs from embryonic stem cells (ESCs) were autonomous in their ability to generate cyst-like organoids. The OVs formed large cysts containing sensory hair cells days after isolation, but the efficiency was dependent on supplementation with the basement membrane matrix Matrigel.

2. Materials and methods

2.1. Mouse ESC maintenance and differentiation

R1/E mouse ESCs (ATCC) were maintained in 1:1 Advanced DMEM/ F12 (Thermo Fisher) and Neurobasal (Thermo Fisher) supplemented with 1× B27 without vitamin A (Thermo Fisher), 0.5× N2 (Thermo Fisher), 1× Glutamax (Thermofisher), 1000U/mL Leukemia Inhibitory Factor (LIF, Thermo Fisher), 3 μM CHIR99021 (Stemcell Technologies), and 1 μM PD0325901 (Stemcell Technologies). The inner ear organoid differentiation protocol, illustrated in Fig. 1A, was modified from prior reports (Koehler et al., 2013, DeJonge et al., 2016, Schaefer et al., 2018). On day 0 (D0), Cells were dissociated using TrypLE (Thermo Fisher) and plated at a concentration of 3,000 cells/well in a round-bottomed 96-well Nunclon Sphera Microplate (Thermo Fisher) containing GMEM (Invitrogen), 1.5% KnockOut serum replacement (Invitrogen), 15 mM HEPES (Invitrogen),

Author Manuscript Author Manuscript Author Manuscript Author Manuscript

1× nonessential amino acids (Invitrogen), 1 mM sodium pyruvate (Invitrogen), and 0.1 mM β-mercaptoethanol (Sigma). On D1, the media was supplemented with 2% v/v Growth Factor Reduced Matrigel (Corning, referred to throughout as Matrigel). On D3, 10 ng/mL BMP4 (Stemgent) and 1 μM Repsox (Tocris) and on D4.25, 1 μM LDN193189 (Stemgent) and 100 ng/mL FGF2 (Sigma) were added to each well. On D8, aggregates were transferred to a new 96-well microplate with 200 μL maturation media (MM: Advanced DMEM/F12, 1× N2, 15 mM HEPES, and 1× Glutamax) with 1% v/v Matrigel and 3 μM CHIR99021. From D10 onwards, half of the media was exchanged for fresh MM each day.

2.2. Vesicle isolation and embedding in Matrigel

D10–14 aggregates were washed with DMEM/F12 and transferred to a low-attachment dish with 1× collagenase/hyaluronidase (Stemcell Technologies). Aggregates were incubated at 37 °C for 45 min and mechanically disrupted every 15 min. After 45 min, aggregates were disrupted with an uncut 1 mL pipet tip and reverse filtered through a 40 μm strainer (Thermo Fisher) into a low-attachment dish using DMEM/ F12. Vesicles were manually collected within 30 min of disruption and transferred into droplets of 100% Matrigel covered in MM or into MM supplemented with lower concentrations of non-polymerized Matrigel.

2.3. Morphology

Brightfield images were taken using a Leica DM IL microscope. Images were analyzed using ImageJ (Schindelin et al., 2012). Diameter and thickness of vesicles was measured every other day. Diameter was calculated as the average of the major axis and its orthogonal while thickness was the average of 4 measurements where the major axis and its orthogonal intercepted the epithelium. Vesicles were excluded from measurements if: i) the center of the vesicle-like object was opaque, ii) debris obscured ability to define inner and outer epithelial boundaries, and/or iii) the vesicle structure was incomplete (i.e. <50% circular). Student's *t*-test for comparison between means and one- and two-way analysis of variance (ANOVA) with Tukey's post-hoc tests were performed using Systat 12.

2.4. Immunohistochemistry

Wholemount cysts from late-stage aggregates were collected, fixed in 4% paraformaldehyde (PFA) for 1 h at room temperature, and washed with phosphate buffered saline (PBS). Wholemount cysts from isolated vesicle cultures were washed in PBS and extracted from the Matrigel by applying Cell Recovery Solution (Corning) for 1 h on ice before fixation as above. Cryosections of late-stage aggregates were stained to illustrate the fine structure of the organoid sensory epithelium. For these preparations, the aggregates were fixed in 4% PFA and cryopreserved in sequential 30 min incubations in 10%, 20%, and 30% sucrose. After overnight exposure to 1:1 mixture of 30% sucrose and O.C.T. embedding compound (ThermoFisher), aggregates were frozen in O.C.T. and 10 μm serial sections collected on SuperFrost Plus slides (ThermoFisher). All samples were blocked and permeabilized in 5% Normal Donkey Serum (Jackson Immuno Research) and 0.1% Triton X-100 in PBS for 15 min. Incubation in primary antibody occurred in blocking and permeabilization buffer overnight at 4 °C. The following primary antibodies were used: MyoVIIa (1:100, Proteus 25–6790), Sox2 (1:100, Santa Cruz SC-365823), Ecad (1:250, BD Biosciences 610181), Laminin (1:500, Abcam AB11575), and Collagen IV (1:200, Chemicon AB756P).

Author Manuscript Author Manuscript Author Manuscript Author Manuscript

Following incubation in primary antibody, cysts were washed with PBS and incubated in Alexa Fluor secondary antibody (1:500; ThermoFisher) and phalloidin fluorescent-conjugate (1:200; Invitrogen) in PBS for 1 h at room temperature. Nuclei were counterstained with Hoechst 33,342 in PBS for 5 min at room temperature. Fluorescent images were taken using an Olympus BX51 microscope with ORCA R2 CCD camera and Metamorph acquisition software for epifluorescence or Leica TCS SP5 for confocal microscopy.

3. Results

3.1. Generation of otic intermediates in large, heterogeneous aggregates

Conventional inner ear organoids and their otic intermediates were generated using the paradigm illustrated in Fig. 1A. Suspensions of mouse ESCs were induced to form compact aggregates (Fig. 1B) and then treated with various chemical cues to form a layer of non-neural ectoderm/otic epibranchial placode (Fig. 1C), as described previously (Koehler et al., 2013, Schaefer et al., 2018). Otic-like vesicles were apparent by D10 and protruding cysts from D18 onward (Fig. 1D, E). Cryosections through the organoids revealed a sensory epithelium with MyoVIIa+ hair cells containing apical hair bundles extending into the lumen of the cyst (Fig. 1F) and positioned atop a layer of Sox2+ supporting cells (Fig. 1G).

3.2. Isolated OVs adopt a cyst-like morphology

Otic intermediates could be isolated from the large cell aggregates starting on D10. Many D10 otic vesicle-like structures were incomplete and resembled otic cups that were at least intact hemispheres (37%). Otic cup isolates formed full vesicles within 2 days of additional culture and could adopt a cyst-like morphology (Fig. S1). Some of these OVs or otic cups maintained a thick vesicular epithelium and showed limited growth over 8 additional days in culture (D10 + 8) (Fig. 2A), while others adopted a cyst-like morphology by growing in diameter with a thinned epithelium (Fig. 2B). About 35% of the D10 OVs could not be tracked over time because they developed into complex structures with dense outgrowths or numerous epithelial folds, preventing downstream morphological analysis (Fig. S2).

We grouped these D10 cultures into cyst and non-cyst categories based on growth and development of a thin epithelium. Mean diameter was determined from measurements along major and minor axes, and mean thickness was determined from four measurements made at the intersections of these axes with the epithelium (Fig. 2C). From 16 preparations observed over time, 10 were classified as cysts and 6 as non-cysts. Mean diameter increased at a faster rate for cysts compared to non-cysts, though each group showed significant changes in growth (one-way ANOVA for each, $P < 0.05$) (Fig. 2D). The ratio of thickness: diameter decreased over time for cysts (one-way ANOVA, $P < 0.01$), consistent with an increasing diameter and thinning epithelium, but the non-cysts showed no systematic change over time (one-way ANOVA, $P = 0.10$) (Fig. 2E). The cysts appeared to grow in diameter without reaching a plateau in this time frame, suggesting ongoing cell division. Cysts derived from isolated OVs contained epithelial layers of MyoVIIa+ hair cells and Sox2 + supporting cells (Fig. 2F). Actin-rich hair bundles extended from the surface of MyoVIIa+ hair cells in organoids derived from isolated OVs (Fig. 2G), like those produced by OVs cultured within the large, complex aggregates of typical organoid cultures (Fig. 2H).

Author Manuscript Author Manuscript Author Manuscript Author Manuscript

3.3. Organoid production efficiency increases at later isolation timepoints

To objectively classify morphological changes, the diameter and epithelial thickness of fresh OV isolates (D10 and D12; N = 119) were compared to late-stage cultures containing a mixture of large cysts and small vesicles (D18′: D10 + 8, D12 + 6, D14 + 4; N = 121). The fresh isolates provided a standard reference for the variation in OV morphology. A histogram of thickness:diameter for these two groups is shown in Fig. 3A. We determined a cutoff of 0.11 at the junction of these groups, with lower values representing cysts and higher values representing non-cysts similar in size and thickness to OV isolates. By D18′, 90% of isolated vesicles had a decreased thickness:diameter ratio compared to fresh vesicle isolates, consistent with their classification as cysts. Classification using this objective method matched subjective determinations from two independent observers (correlation coefficient greater than 0.9 for each).

Using this classification scheme, we assessed OV morphology and the efficiency of cystic organoid production in D10 isolates (i.e. the earliest stage of OV formation) up to D14 (i.e. when OVs express the pro-sensory gene Atoh1, (DeJonge et al., 2016)). Even though some larger protrusions could be observed in intact aggregates at D14, these did not survive the trituration and vesicle isolation procedures, leading to selection of OVs with similar morphology regardless of starting stage (Fig. 3B-D; one-way ANOVA, $P = 0.08$). A majority (greater than 70%) of vesicles isolated at D10 adopted a cyst-like morphology, suggesting that competency for organoid-genesis is determined early. Vesicles isolated on D12 or after achieved over 90% efficiency in cyst formation, often producing cysts after only 2 days in culture (Fig. 3C-D). Therefore, even though we isolated tissues with similar size and shape at each time point, efficiency of organoid production was better with the later stage OVs.

To determine whether these results extended to other cell lines, we repeated the approach using Atoh1nGFP and Fbxo2-VHC ESCs. Each of these lines has been used previously to make inner ear organoids (Liu et al., 2016, Hartman et al., 2018). Both lines produced organoids in D20 aggregate cultures (Fig. S3A, C) and from OVs isolated on D12 and cultured to D12 + 6 (Fig. S3B, D). These additional cell lines produced organoids with similar average diameters to the R1/E cultures (Fig. S3E; one-way ANOVA, $P = 0.06$) and similar thickness:diameter ratios (Fig. S3F; one-way ANOVA, $P = 0.34$). The efficiency of organoid production was somewhat lower than controls (i.e. R1/E 91%, Atoh1nGFP 71%, Fbxo2-VHC 83%), but these differences were not statistically significant (Chi-squared test, $P = 0.17$).

3.4. Organoid production efficiency decreases with decreasing Matrigel concentration

To determine the impact of Matrigel on organoid-genesis, vesicles were isolated at D12 and cultured in MM supplemented with 0% to 10% Matrigel. By D12 + 6, a relatively high organoid efficiency and low thickness:diameter ratio was found for cultures in as low as 1% Matrigel (Fig. 4A). Fitting efficiency to a modified Hill equation, where Efficiency = ($Efficiency_{max}$ * [Matrigel]) / (EC_{50} + [Matrigel]), resulted in an effective concentration of 0.2% Matrigel to produce about 50% cystic organoids (EC_{50}). The size and shape of organoids produced in 0.1% to 100% Matrigel were similar (Fig. 4B). Even though 0.1% Matrigel resulted in a lower efficiency of organoid-genesis, these cysts still contained

Author Manuscript Author Manuscript Author Manuscript Author Manuscript

MyoVIIa+ hair cells (Fig. 4C). In cultures without Matrigel supplementation, OV growth was stunted, and no cystic organoids were produced.

3.5. Deposition of ECM around D12 OVs

Matrigel is primarily composed of the ECM proteins laminin, collagen IV, and entactin (Kleinman et al., 1986), suggesting that these protein components may regulate organoid-genesis from isolated OVs. Since laminin and collagen are essential components of the native OV in vivo (Krotoski et al., 1986, Hilfer and Randolph, 1993, Visconti and Hilfer, 2002, Barrionuevo et al., 2008), we examined the deposition of laminin and collagen IV in organoid cultures. Laminin was found throughout the aggregate with heavy deposition around the OVs (Fig. 4D). Collagen IV was found primarily associated with the outer epithelium of the aggregate but was also lightly deposited around the OV (Fig. 4E).

4. Discussion

Conventional inner ear organoid protocols suffer from variability and inefficiency. In estimates from a standard inner ear organoid protocol, about 15–25 OVs can be obtained per aggregate but only 3–6 organoids are produced (Koehler and Hashino, 2014). However, when OVs were isolated from the aggregates and grown in the absence of nonotic cells, nearly every OV was capable of differentiating into a cystic organoid. Interestingly, genetic background appears to influence differentiation efficiency in conventional organoid protocols (Tang et al., 2019). While the bulk of our analysis was completed on the R1/E cell line, which is from a mixed 129X1/129S1 mouse strain, we obtained similar results from additional cell lines from different backgrounds (i.e. Atoh1nGFP from C57BL/6 × DBA/2 hybrids and Fbxo2-VHC from 129/ Ola). Thus, organoid-genesis from isolated OVs is autonomous, relying on an intrinsic differentiation program, and this process appears to be independent of genetic background.

Early isolates from D10 cultures produced cystic organoids with moderate efficiency (~70%) and were prone to generating complex morphologies and dense outgrowths. The nature of these outgrowths remains to be determined, but it is possible that D10 OVs included progenitors with greater differentiation potential. We previously showed that Islet1-positive neuroblasts delaminate from the OVs by D12 (Schaefer et al., 2018). Thus, isolation of OVs at early time points may favor neurogenesis as well as formation of sensory epithelia, resulting in greater complexity.

Our results are similar to those from animal-derived OVs, which fail to develop into sensory epithelial tissues in the absence of ECM support (Garrido et al., 1998) but generate complex morphologies reminiscent of sensory epithelia when grown in Matrigel (Miura et al., 2004). Though Matrigel is essential to efficient organoid-genesis, its role is unclear. This matrix is a complex mixture of ECM proteins (i.e. ~ 60% laminin, ~30% collagen IV, and ~ 8% entactin) and several growth factors (Corning, Kleinman et al., 1986). Batch-to-batch variability in Matrigel composition has been frequently associated with variable outcomes in organoid protocols (Tian et al., 2020). Over 1,000 unique proteins have been identified in Matrigel with considerable batch-to-batch variability in protein content (Hughes et al., 2010).

Author Manuscript Author Manuscript Author Manuscript Author Manuscript

The major growth factors in Matrigel are IGF-1, TGFβ, and VEGF (Corning. Corning Matrigel Matrix, 2019). However, the concentration of these factors in 0.2% Matrigel—the EC_{50} for organoid-genesis—is quite low, on the order of 1 pg/mL. It is unlikely that the low concentrations of growth factors found in Matrigel are substantially impacting organoid-genesis. Instead, the ECM components within Matrigel likely influence organoid-genesis. Several developmental studies point to the importance of laminin, collagen, and fibronectin in OV morphogenesis (Krotoski et al., 1986, Hilfer and Randolph, 1993, Visconti and Hilfer, 2002). Studies of mouse inner ear development also show laminin deposition around the otic placode and OV (Barrionuevo et al., 2008). Injection of function-blocking antibodies to laminin resulted in dysmorphogenesis of otic tissue in vivo; injections of blocking antibodies to integrin receptors that bind laminin had similar, though less severe, effects (Visconti and Hilfer, 2002). Laminin was also heavily deposited around stem cell-derived OVs within the larger cellular aggregates. Taken together, laminin is a strong candidate for playing a role in OV-to-organoid maturation.

The generation of inner ear organoids from pluripotent stem cells holds great promise for unraveling the complexities of sensory tissue development, disease, pharmacological treatments, and regeneration. The autonomy of OV morphogenesis and differentiation into sensory epithelia suggests that the D12-D14 OVs are suitable donor material for regenerative medicine approaches in the severely damaged inner ear where replacement of both sensory and non-sensory cells is required. The culture of isolated, stem cell-derived OVs also opens the door to new approaches to guide cell fate and mimic the axial patterning in normal inner ear development. Axial patterning is essential for defining sensory and non-sensory domains as well as cochlear and vestibular domains. However, it is difficult to recapitulate the morphogenic gradients that guides this patterning in the typical organoid cultures with intact whole aggregates. Combining our approach with microfluidics will open new paths to exploring patterning in stem cell-derived otic mimetics.

Supplementary Material

Refer to Web version on PubMed Central for supplementary material.

Acknowledgements

The authors thank Andrew Wylie for assistance with morphological assessments and Mitchell Fruchtman for assistance with ECM immunofluorescence staining, as well as funding support from NIH NIDCD (R21 DC016171 to R.K.D.) and the University of Michigan Program in Biological Sciences fellowship funds to S.E.H.

References

Barrionuevo F, Naumann A, Bagheri-Fam S, Speth V, Taketo MM, Scherer G, Neubüser A, 2008. Sox9 is required for invagination of the otic placode in mice. Dev. Biol. 317, 213–224. [PubMed: 18377888]

Corning. Corning Matrigel Matrix. https://www.corning.com/catalog/cls/documents/faqs/CLS-DL-CC-026.pdf, Last accessed on: 6/1/2019.

DeJonge RE, Liu X-P, Deig CR, Heller S, Koehler KR, Hashino E, 2016. Modulation of Wnt Signaling Enhances Inner Ear Organoid Development in 3D Culture. PLoS ONE11, e0162508. [PubMed: 27607106]

Author Manuscript Author Manuscript Author Manuscript Author Manuscript

Dye BR, Hill DR, Ferguson MA, Tsai YH, Nagy MS, Dyal R, Wells JM, Mayhew CN, Nattiv R, Klein OD, White ES, Deutsch GH, Spence JR, 2015. In vitro generation of human pluripotent stem cell derived lung organoids. Elife4, e05098.

Eiraku M, Takata N, Ishibashi H, Kawada M, Sakakura E, Okuda S, Sekiguchi K, Adachi T, Sasai Y, 2011. Self-organizing optic-cup morphogenesis in three-dimensional culture. Nature472, 51–56. [PubMed: 21475194]

Eiraku M, Watanabe K, Matsuo-Takasaki M, Kawada M, Yonemura S, Matsumura M, Wataya T, Nishiyama A, Muguruma K, Sasai Y, 2008. Self-organized formation of polarized cortical tissues from ESCs and its active manipulation by extrinsic signals. Cell Stem Cell3, 519–532. [PubMed: 18983967]

Garrido JJ, Schimmang T, Represa J, Giraldez F, 1998. Organoculture of otic vesicle and ganglion. Curr. Top Dev. Biol. 36, 115–131. [PubMed: 9342524]

Hartman BH, Böscke R, Ellwanger DC, Keymeulen S, Scheibinger M, Heller S, 2018. Fbxo2VHC mouse and embryonic stem cell reporter lines delineate in vitro-generated inner ear sensory epithelia cells and enable otic lineage selection and Cre-recombination. Dev. Biol. 443, 64–77. [PubMed: 30179592]

Hilfer SR, Randolph GJ, 1993. Immunolocalization of basal lamina components during development of chick otic and optic primordia. Anat. Rec. 235, 443–452. [PubMed: 8430914]

Huch M, Knoblich JA, Lutolf MP, Martinez-Arias A, 2017. The hope and the hype of organoid research. Development144, 938–941. [PubMed: 28292837]

Hughes CS, Postovit LM, Lajoie GA, 2010. Matrigel: a complex protein mixture required for optimal growth of cell culture. Proteomics10, 1886–1890. [PubMed: 20162561]

Kleinman HK, McGarvey ML, Hassell JR, Star VL, Cannon FB, Laurie GW, Martin GR, 1986. Basement membrane complexes with biological activity. Biochemistry25, 312–318. [PubMed: 2937447]

Koehler KR, Hashino E, 2014. 3D mouse embryonic stem cell culture for generating inner ear organoids. Nat. Protoc. 9, 1229–1244. [PubMed: 24784820]

Koehler KR, Mikosz AM, Molosh AI, Patel D, Hashino E, 2013. Generation of inner ear sensory epithelia from pluripotent stem cells in 3D culture. Nature500, 217–221. [PubMed: 23842490]

Krotoski DM, Domingo C, Bronner-Fraser M, 1986. Distribution of a putative cell surface receptor for fibronectin and laminin in the avian embryo. J. Cell Biol. 103, 1061–1071. [PubMed: 2943743]

Liu XP, Koehler KR, Mikosz AM, Hashino E, Holt JR, 2016. Functional development of mechanosensitive hair cells in stem cell-derived organoids parallels native vestibular hair cells. Nat Commun7, 11508. [PubMed: 27215798]

McCracken KW, Cata EM, Crawford CM, Sinagoga KL, Schumacher M, Rockich BE, Tsai YH, Mayhew CN, Spence JR, Zavros Y, Wells JM, 2014. Modelling human development and disease in pluripotent stem-cell-derived gastric organoids. Nature516, 400–404. [PubMed: 25363776]

Miura T, Shiota K, Morriss-Kay G, 2004. A mesenchyme-free culture system to elucidate the mechanism of otic vesicle morphogenesis. J. Anat. 205, 297–312. [PubMed: 15447689]

Schaefer SA, Higashi AY, Loomis B, Schrepfer T, Wan G, Corfas G, Dressler GR, Duncan RK, 2018. From Otic Induction to Hair Cell Production: Pax2EGFP Cell Line Illuminates Key Stages of Development in Mouse Inner Ear Organoid Model. Stem Cells Dev. 27, 237–251. [PubMed: 29272992]

Schindelin J, Arganda-Carreras I, Frise E, Kaynig V, Longair M, Pietzsch T, Preibisch S, Rueden C, Saalfeld S, Schmid B, Tinevez JY, White DJ, Hartenstein V, Eliceiri K, Tomancak P, Cardona A, 2012. Fiji: an open-source platform for biological-image analysis. Nat Methods9, 676–682. [PubMed: 22743772]

Spence JR, Mayhew CN, Rankin SA, Kuhar MF, Vallance JE, Tolle K, Hoskins EE, Kalinichenko VV, Wells SI, Zorn AM, Shroyer NF, Wells JM, 2011. Directed differentiation of human pluripotent stem cells into intestinal tissue in vitro. Nature470, 105–109. [PubMed: 21151107]

Taguchi A, Kaku Y, Ohmori T, Sharmin S, Ogawa M, Sasaki H, Nishinakamura R, 2014. Redefining the in vivo origin of metanephric nephron progenitors enables generation of complex kidney structures from pluripotent stem cells. Cell Stem Cell14, 53–67. [PubMed: 24332837]

Author Manuscript Author Manuscript Author Manuscript Author Manuscript

Tang P-C, Alex AL, Nie J, Lee J, Roth AA, Booth KT, Koehler KR, Hashino E, Nelson RF, 2019. Defective Tmprss3-Associated Hair Cell Degeneration in Inner Ear Organoids. Stem Cell Reports13, 147–162. [PubMed: 31204303]

Tian A, Muffat J, Li Y, 2020. Studying Human Neurodevelopment and Diseases Using 3D Brain Organoids. J. Neurosci. 40, 1186–1193. [PubMed: 32024767]

Visconti RP, Hilfer SR, 2002. Perturbation of extracellular matrix prevents association of the otic primordium with the posterior rhombencephalon and inhibits subsequent invagination. Dev. Dyn. 223, 48–58. [PubMed: 11803569]

Author Manuscript Author Manuscript Author Manuscript Author Manuscript

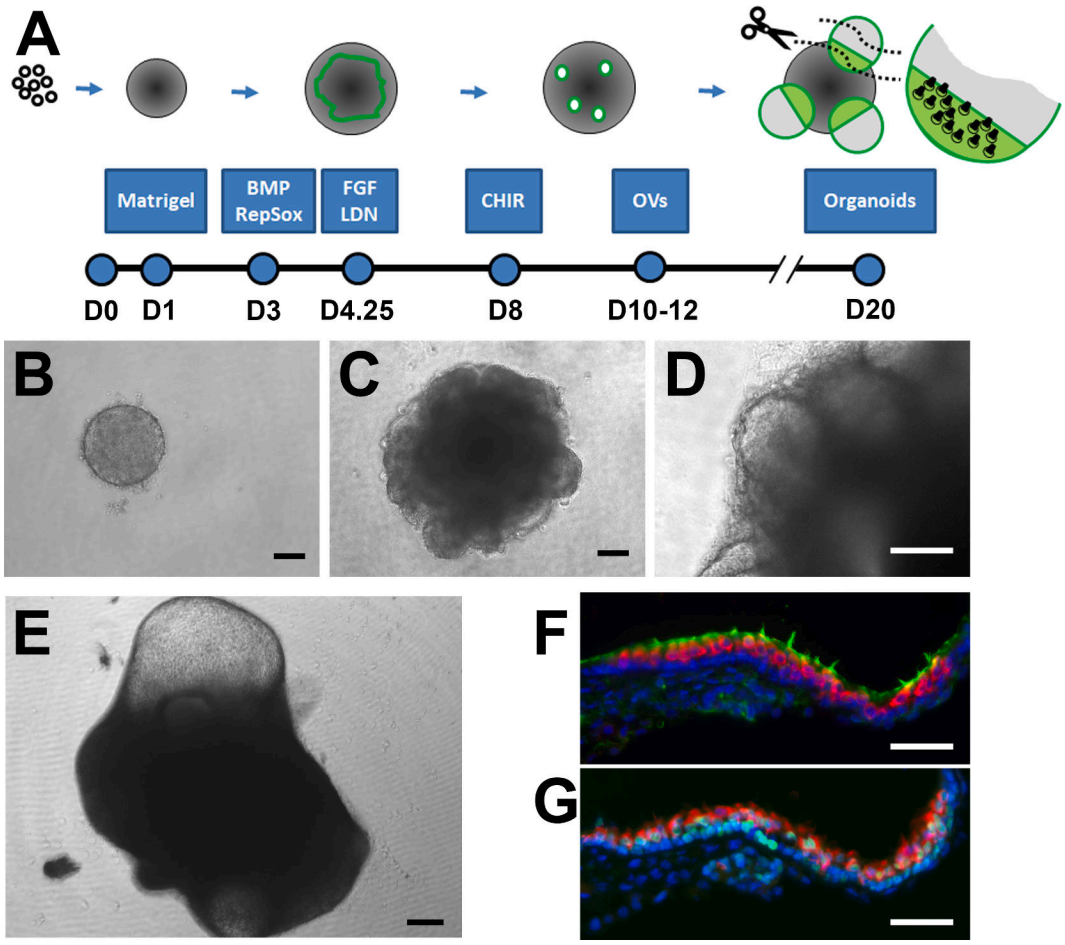

Fig. 1.

Generation of otic intermediates and inner ear organoids from mouse ESCs. (A) Illustration of the culture paradigm notes chemical cues provided at key time points along with major developmental milestones. (B) Aggregates of ESCs are exposed to 2% Matrigel on D1 to induce epithelial formation and (C) treated with chemical cues to induce the formation of a ruffling non-neural ectoderm/otic epibranchial placode evident on D6. (D) OVs are apparent by D10 and (E) protruding cysts from D18 onward (D19 aggregate shown). Sensory hair cells are found at the boundary of the cyst and larger aggregate, shown in neighboring cryosections labeled with (F) MyoVIIa + sensory cells (red) with phalloidin + hair bundles (green) and (G) MyoVIIa hair cells (red) among Sox2 + supporting cells (green) (counterstained with Hoechst in blue). Scale bars: B-D, 100 μm; E, 200 μm; F-G, 50 μm.

Author Manuscript Author Manuscript Author Manuscript Author Manuscript

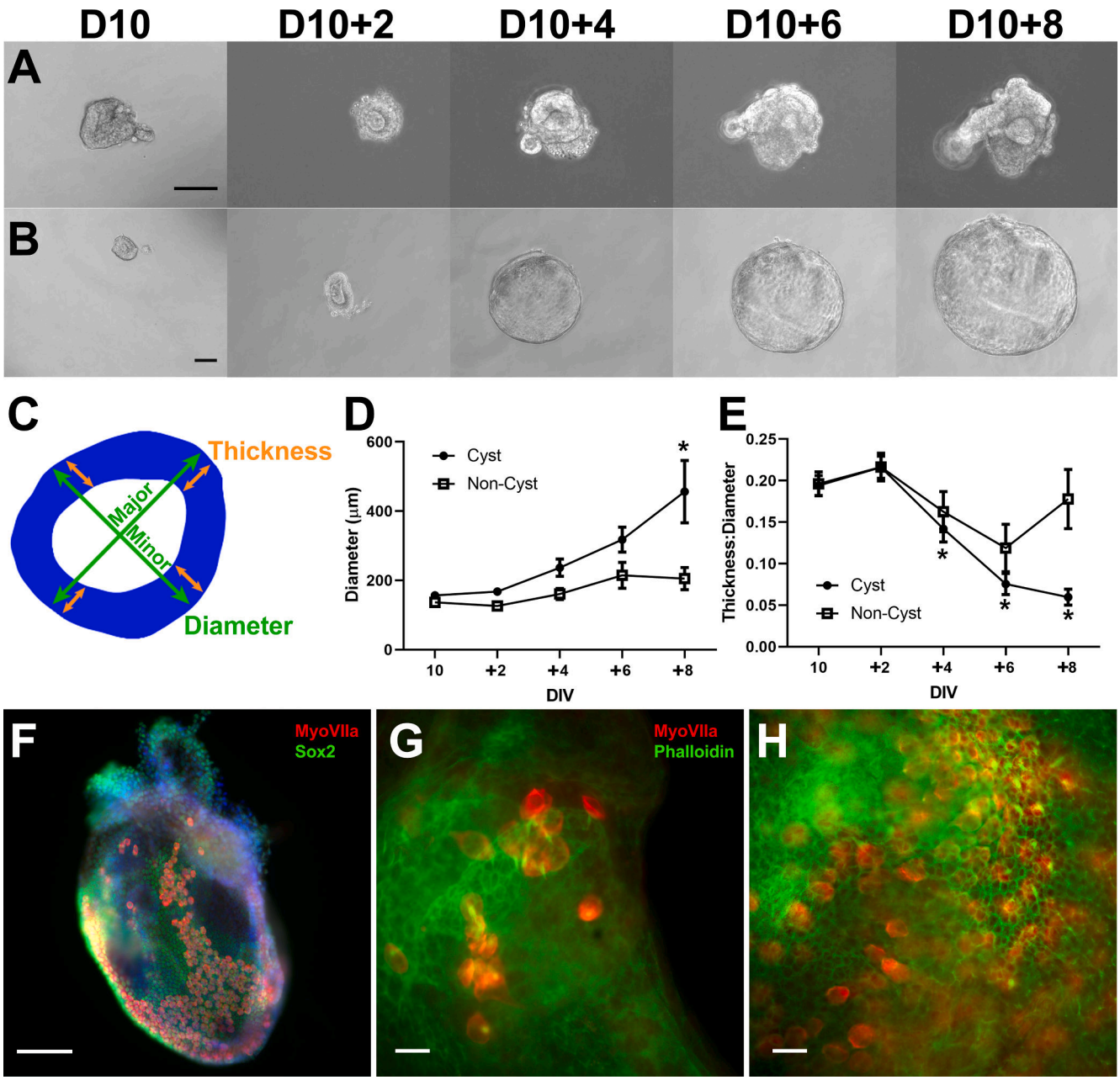

Fig. 2.

Cysts generated by isolated vesicles are inner ear organoids. (A) Example of D10 OV culture for 8 days showing minimal growth. (B) Example of D10 OV culture developing into a large, thin cyst-like structure. Cultures were subjectively divided into cyst and non-cyst based on morphology of endpoints. (C) Illustration of morphological measurements, with epithelium (blue) derived from an outline of a D12 + 2 preparation. Diameter was measured along major and minor axes (green arrows) and averaged. Epithelial thickness was measured at four locations (orange arrows) at intersections of the major and minor axes and averaged. The average diameter (D) and thickness:diameter ratio (E) are shown for cyst (N = 10) and non-cyst (N = 6) cultures (* $P < 0.05$ post-hoc Tukey-HSD analysis compared to D10 for

Author Manuscript Author Manuscript Author Manuscript Author Manuscript

each group). Error bars represent one standard error of the mean. (F) D12 + 4 cyst contains hundreds of MyoVIIa+ sensory hair cells (red) among Sox2+ supporting cells (green). (G) D12 + 6 wholemount cyst showing MyoVIIa+ sensory cells (red) with phalloidin+ hair bundles (green) extending into the lumenal space of the cyst (representative of 10 preparations from 3 separate cultures), similar to preparations from intact D18 aggregates (H). Scale bars: A-B,E-F: 100 μm; G-H: 20 μm.

Author Manuscript Author Manuscript Author Manuscript Author Manuscript

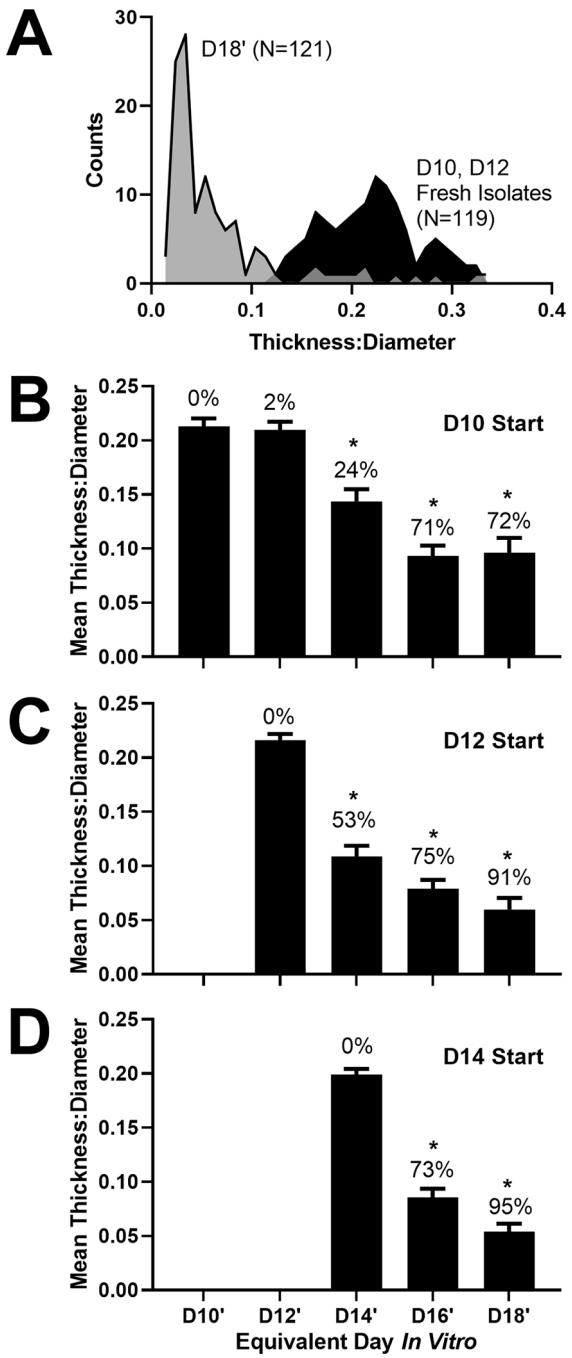

Fig. 3.

Impact of start date on the change in vesicle morphology over time. (A) Histogram of the morphology of fresh vesicle isolates and long-term cultures in 100% Matrigel. Thickness:diameter ratio is reported for fresh vesicle isolates from D10 and D12 aggregate cultures (N = 119) and from long-term cultures at equivalent culture D18 (N = 121; D18′, from D10 + 8, D12 + 6, D14 + 4 groups). Measurements were made from more than 10 independent cultures in each group. (B)-(D) The mean thickness:diameter ratio is shown for OVs isolated from D10, D12, and D14 aggregates and cultured in droplets of 100%

Author Manuscript Author Manuscript Author Manuscript Author Manuscript

Matrigel. Error bars represent one standard error of the mean. The percentage of vesicles adopting a cyst-like shape, based on a ratio cutoff of 0.11, is shown above each bar. *, $P < 0.01$ for Tukey-HSD post-hoc test compared to the day of isolation. Sample sizes per group: (B) D10 N = 44, D10 + 2 N = 40, D10 + 4 N = 38, D10 + 6 N = 35, D10 + 8 N = 32; (C) D12 N = 78, D12 + 2 N = 74, D12 + 4 N = 72, D12 + 6 N = 34; (D) D14 N = 75, D14 + 2 N = 62, D14 + 4 N = 44.

Author Manuscript Author Manuscript Author Manuscript Author Manuscript

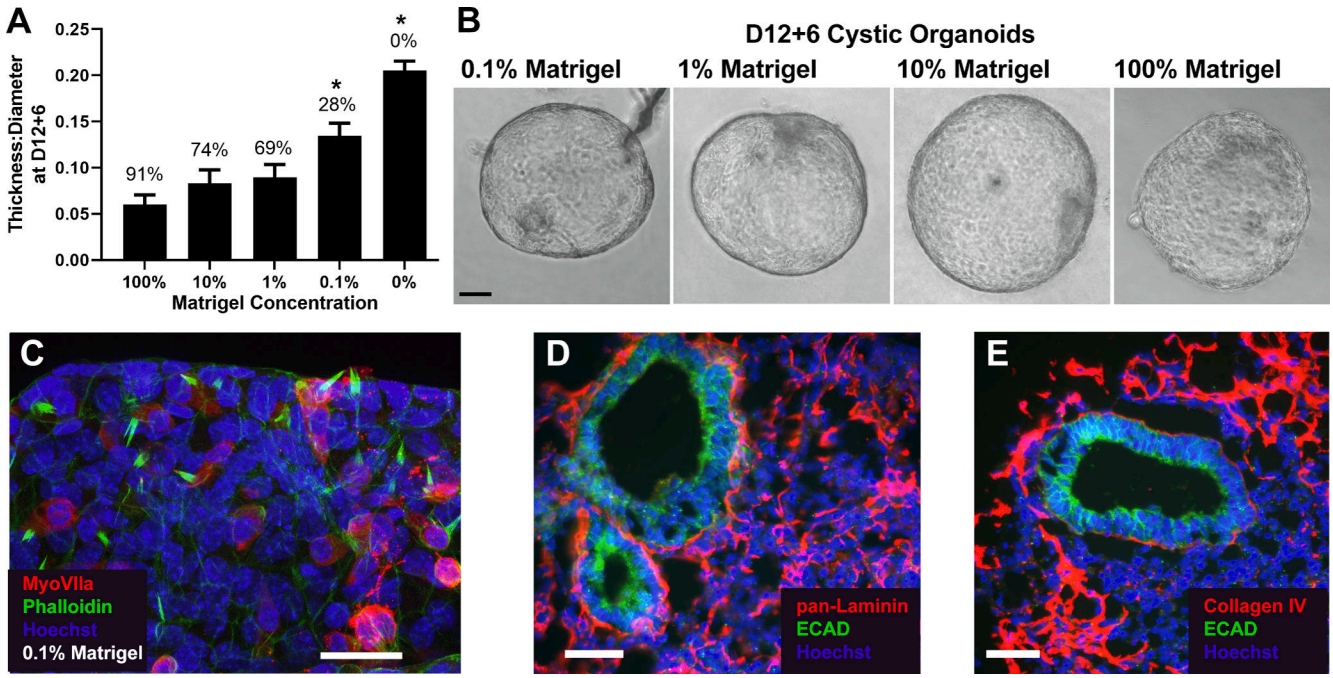

Fig. 4.

Impact of Matrigel concentration on cyst production. (A) Mean thickness:diameter ratio at D12 + 6 for vesicles cultured in media supplemented with 0%-10% Matrigel. Assessments were made from at least 3 independent experiments in each group. Data are shown compared to 100% Matrigel from Fig. 3. Error bars represent one standard error of the mean. *, $P < 0.01$ from post-hoc Tukey-HSD test compared to control 100% Matrigel. Sample sizes per group at D12 + 6: 0% Matrigel N = 37, 0.1% Matrigel N = 18, 1% Matrigel N = 26, 10% Matrigel N = 35. (B) Exemplary images of cystic organoid at D12 + 6 in each Matrigel condition, except 0% Matrigel, which did not generate any cysts. (C) D12 + 6 cyst cultured in 0.1% Matrigel with cells expressing the hair cell marker MyoVIIa (red) and phalloidin+ hair bundles (green), counterstained with Hoechst (blue). Image is representative of 5 cysts under these conditions. Cryosections from D12 aggregates were immunostained for (D) pan-laminin and (E) collagen IV (red) and counterstained with Ecad to identify the OVs (green) and Hoechst to label nuclei. Laminin and collagen IV are shown deposited on and around the OVs. Images are representative of over 25 OVs from more than 10 individual aggregates in 2 separate cultures. Scale bars: B: 25 μm; C-D: 50 μm.